Environmental Science & Technology

Article

Cite This: Environ. Sci. Technol. 2019, 53, 10361−10370

pubs.acs.org/est

Unexpectedly Increased Particle Emissions from the Steel Industry Determined by Wet/Semidry/Dry Flue Gas Desulfurization Technologies

Xiang Ding,[†] Qing Li,*[,†,‡] Di Wu,[†] Yingguang Liang,[†] Xianmang Xu,[§] Guangzhao Xie,[†] Yaqi Wei,[†] Hao Sun,[†] Chao Zhu,[†] Hongbo Fu,[†,‡] and Jianmin Chen*[,†,‡,∥]

[†]Shanghai Key Laboratory of Atmospheric Particle Pollution and Prevention, Department of Environmental Science and Engineering, Institute of Atmospheric Sciences, Fudan University, Shanghai 200433, China

[‡]Shanghai Institute of Eco-Chongming (SIEC), No. 3663 Northern Zhongshan Road, Shanghai 200062, China

[§]Biological Engineering Technology Innovation Center of Shandong Province, Shandong Academy of Sciences, Heze 274008, China

[∥]Center for Excellence in Regional Atmospheric Environment, Institute of Urban Environment, Chinese Academy of Sciences, Xiamen 361021, China

Supporting Information

ABSTRACT: "Ultralow-emission" standards have started to be implemented for steel plants in China. Flue gas desulfurization (FGD) systems integrating desulfurization and dedusting, common end-of-pipe technologies before the stacks, have been a key process for controlling the complexity of sintering flue gas to meet ultralow-emission requirements. This study reports comprehensive analysis of the influence of wet/semidry/dry FGD systems on particulate emissions via a field investigation of five typical sinter plants equipped with various FGD devices. The size distribution and mass concentration of particulate matter (PM) are adjusted to different ranges by these FGD systems. Chemical analysis of the PM compositions shows that 20−95% of the mass of inlet PM is removed by FGD systems, while it is estimated that approximately 17, 63, 59, and 71% of the outlet PMs are newly contributed by desulfurizers and their byproducts for the tested wet limestone, wet ammonia, semidry circulating fluidized bed, and activated coke FGD systems, respectively. The newly contributed compositions of $PM_{2.5}$ emitted from these FGD systems are dominated by $CaSO_4$, $(NH_4)_2SO_4$, $CaSO_4$ + CaO, and coke carbon, respectively. These results suggest that the deployment of FGD technology should be comprehensively considered to avoid additional negative impacts from byproducts generated in control devices on the atmosphere.

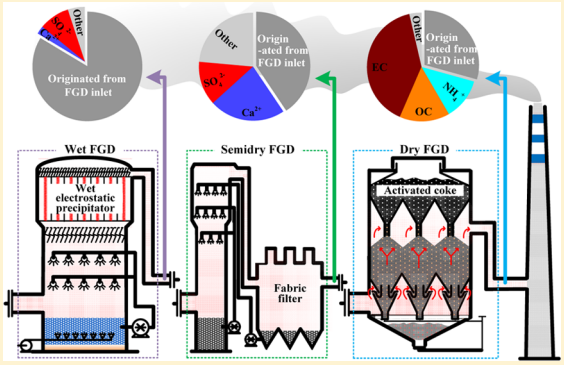

INTRODUCTION

Severe haze pollution associated with fine particulate matter (PM), i.e., $PM_{2.5}$ (PM with an aerodynamic diameter less than 2.5 μm), has frequently occurred in China in the past 2 decades.[1−3] Aiming to reduce PM emissions from anthropogenic sources and improve air quality, the Chinese government has promulgated strict regulations and standards for most major emission sources and updated them every few years. The strictest regulation, also called the "ultralow-emission" standard, has been implemented for pollutant emissions from coal-fired power plants (CFPPs) since 2014.[4] By the end of 2017, approximately 71% of CFPPs had already met the ultralow-emission standard (PM < 10 mg/Nm^3, SO_2 < 35 mg/Nm^3, and NO_x < 50 mg/Nm^3) by employing various ultralow-emission technologies. Ultralow-emission technologies for high-capacity CFPPs mainly include selective catalytic reduction (SCR), electrostatic precipitators (ESPs), and flue gas desulfurization (FGD) combined with wet ESPs, while air pollution control devices (APCDs) for low-capacity CFPPs are more diverse, including circulating fluidized bed (CFB)-FGD, selective noncatalytic reduction (SNCR), electrostatic fabric filters (FFs), and semidry limestone FGD.[5−9] As a benefit of the ultralow-emission standard, the amounts of the pollutants PM, SO_2, and NO_x emitted from CFPPs in 2017 were approximately 18.6, 70.0, and 46.8% less than those in 2013, respectively.[10]

Pollutant emissions from the nonpower industry have recently attracted increasing attention as CFPPs have significantly reduced their emissions, especially those from one of the major industrial sources, i.e., steel plants.[11−13] A total of 17.1−36.9% of the atmospheric $PM_{2.5}$ in many

Received: May 23, 2019
Revised: July 27, 2019
Accepted: August 8, 2019
Published: August 8, 2019

DOI: 10.1021/acs.est.9b03081
Environ. Sci. Technol. 2019, 53, 10361−10370

Table 1. Information on the Sampling Sites and Parameters of Flue Gases[a]

sampling sites	P1				P2	
	sinter-1,2,3	sinter-1	sinter-2	sinter-3	sinter-4	sinter-5
APCDs	ESP	ESP + L-WFGD + WESP	ESP + A-WFGD + WESP	ESP + AC-FGD	ESP + CFB-FGD + FF	ESP + CFB-FGD + FF
collection location	FGD inlet	stack	stack	stack	stack	stack
T (°C)	147 ± 2	55 ± 1	54 ± 1	121 ± 2	79 ± 1	82 ± 1
Q (10^4 Nm^3/h)	44 ± 4	103 ± 2	102 ± 4	149 ± 3	204 ± 4	240 ± 3
AWC (g/Nm^3)	56 ± 4	124 ± 14	116 ± 3	82 ± 6	92 ± 5	96 ± 10
O_2 (%)	17.3 ± 0.1	16.4 ± 0.1	17.1 ± 0.1	15.6 ± 0.1	16.2 ± 0.2	17.1 ± 0.3
CO_2 (%)	3.13 ± 0.02	4.52 ± 0.01	3.29 ± 0.06	4.78 ± 0.04	4.19 ± 0.07	4.23 ± 0.05
CO (g/Nm^3)	6.21 ± 2.76	5.05 ± 2.31	6.16 ± 2.79	4.50 ± 2.01	5.67 ± 1.54	5.78 ± 2.11
NO_x (mg/Nm^3)	137 ± 7	158 ± 3	146 ± 10	34 ± 1	123 ± 14	115 ± 18
SO_2 (mg/Nm^3)	672 ± 35	73 ± 8	64 ± 21	36 ± 5	57 ± 12	49 ± 6
SO_3 (mg/Nm^3)	0.57 ± 0.09	0.25 ± 0.06	3.68 ± 0.20	0.23 ± 0.10	N.S.	N.S.
HCl (mg/Nm^3)	20.31 ± 3.34	0.86 ± 0.25	0.44 ± 0.13	0.56 ± 0.09	N.S.	N.S.
NH_3 (mg/Nm^3)	5.51 ± 0.72	0.77 ± 0.21	28.71 ± 17.22	20.13 ± 3.24	N.S.	N.S.
$PM_{2.5}$ (mg/Nm^3)	20.92 ± 6.91	16.83 ± 2.34	13.92 ± 4.41	6.32 ± 1.85	2.15 ± 0.35	0.22 ± 0.06
$PM_{>2.5}$ (mg/Nm^3)	10.12 ± 1.83	3.87 ± 1.69	7.72 ± 2.07	3.98 ± 1.28	10.9 ± 4.7	0.32 ± 0.09
TSP (mg/Nm^3)	31.14 ± 5.72	20.70 ± 4.12	21.61 ± 5.32	10.33 ± 1.30	13.1 ± 2.51	0.54 ± 0.10

[a]"N.S.", no sampling for this gaseous pollutant; L-WFGD, lime-gypsum wet flue gas desulfurization; WESP, wet electrostatic precipitator; A-WFGD, ammonia wet flue gas desulfurization; AC-FGD, activated coke dry flue gas desulfurization; CFB-FGD, circulating fluidized bed semidry flue gas desulfurization; FF, fabric filter; T, flue gas temperature; Q, flue gas flow rate; AWC, absolute water content.

industrial cities has been attributed to emissions from steel plants, as suggested by source apportionment investigations.[14−16] China has been the largest steel producer in the world since 1996 (837.7 Mt in 2017, approximately 49.2% of the total production in the world).[17,18] Figure S1 shows that the relative contribution of primary $PM_{2.5}$ emissions from the steel industry to total anthropogenic emissions grew from 5.4 to 8.2% from 2005 to 2014 in mainland China, while the relative contribution from CFPPs decreased from 9.5 to 5.1% in the same period, mainly attributed to the ultralow-emission requirement. Because steel emission standards lagged behind those for CFPPs during this period, the steel industry has emitted more $PM_{2.5}$ than CFPPs since 2008.[17,18] Aiming to improve local air quality, Hebei Province in North China has implemented an ultralow-emission standard for steel plants starting in 2019.[19] The emission parameters for sinter flue gas in the Hebei ultralow-emission standard are the same as those for CFPPs. Although there is still no national standard for steel plants similar to the ultralow-emission standard for CFPPs deployed in mainland China, the detailed requirements of pollutant emissions for the steel industry have recently been under discussion with regard to standard feasibility and flue gas complexity.

The whole iron and steel producing process, mainly including sintering/pelletizing facilities, blast furnaces, basic oxygen furnaces, electric arc furnaces, and steelmaking furnaces, can generate pollutant emissions.[20,21] The sintering process is the major emission source of most pollutants, including PM, SO_2, and NO_x, with relative contributions of approximately 30−45, 70, and 90%, respectively, in the whole process.[13,22] Sintering flue gases are generally much more complex than those of CFPPs, exhibiting traits such as variable concentrations/compositions of pollutants, including SO_2 and unknown corrosive gases, large temperature fluctuations ranging from 80 to 180 °C, and high variations in oxygen content ranging from approximately 10 to 15%. Owing to these complexities of flue gas, the installed rates of denitrification, dedusting, and desulfurization devices in China's sintering facilities was approximately 2, 100, and 50% in 2015, respectively.[23] Dedusting technology is currently dominated by ESPs, while FGD technologies for sintering flue gases are relatively diverse and are applied as end-of-pipe technologies before the flue gas enters the stack.

Various FGD technologies have been developed for sintering flue gases to meet the further requirements of the ultralow-emission standard, including limestone/ammonia wet FGD (WFGD) systems combined with wet ESPs (WESPs), CFB-FGD systems, and activated carbon FGD systems.[24] According to the water content of the desulfurizing agents, FGD systems can be roughly classified as WFGD (such as limestone/ammonia WFGD), semidry (such as CFB-FGD), and dry (such as activated carbon FGD) technologies. The installation areas of such systems at sintering facilities from 2005 to 2013 in mainland China are shown in Figure S1. WFGD technologies are the most commonly employed technologies in sintering, while limestone WFGD accounts for nearly a half of all installed FGD devices.[11] However, the average desulfurization efficiency of WFGD systems for sintering flue gases is approximately half that of systems equipped in CFPPs.[5] Limestone WFGD devices are reported to increase PM concentrations at the FGD outlet due to new particles generated from escaped desulfurizing slurries during application in CFPPs,[25,26] while installing a WESP combined with WFGD before entering the stack can significantly reduce the PM concentration.[5,26] Therefore, WFGD systems are commonly combined with WESPs to meet the ultralow-

DOI: 10.1021/acs.est.9b03081
Environ. Sci. Technol. 2019, 53, 10361−10370

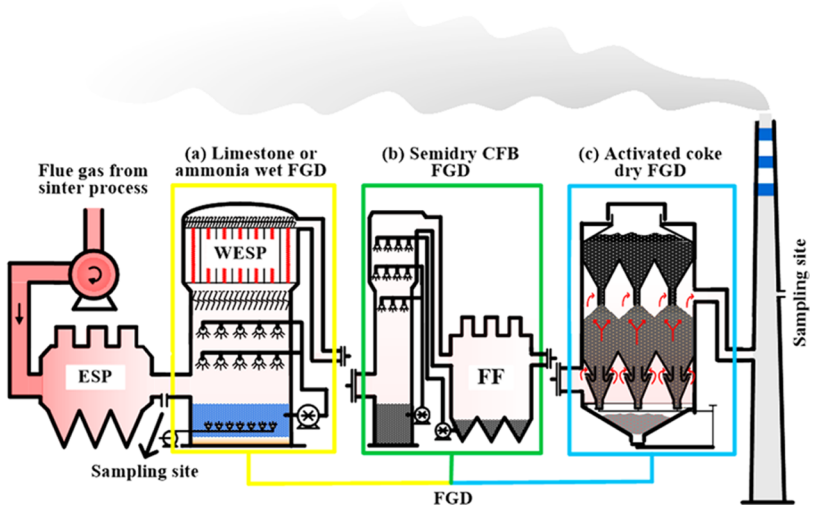

Figure 1. Schematic configuration of APCDs and sampling sites. (a) Limestone and ammonia WFGD system combined with a WESP. (b) Semidry CFB-FGD system combined with an FF. (c) Activated coke dry FGD system.

emission standard (10 mg/Nm^3 for PM) required for CFPPs in mainland China and steel plants in many regions. Semidry FGD systems combined with FFs and dry FGD systems are also installed in many areas with additional functions of denitrification and dedusting (see Figure S1). Although there are a few recent reports on the characteristics of pollutant emissions related to the FGD process with a focus on CFPPs,[5,26] a comprehensive/comparative estimation of various FGD technologies on final pollutant emissions is still lacking, especially their applications in meeting the potential ultralow-emission standard for steel plants. Thus, a systematic estimation of the effect of typical FGD technology on final pollutant emissions is urgently needed to provide scientific evidence for the coming deployment of an ultralow-emission standard for the steel industry.

Aiming to deepen the understanding of the effect of various FGD technologies on final pollutant emissions from the sintering process, this study comparatively investigated gaseous and particulate pollutants treated by FGD technologies. Field measurements of five typical FGD systems (including one limestone WFGD, one ammonia WFGD, two semidry CFB-FGDs, and one activated coke FGD) were conducted with the same sampling and analysis methods. The dedusting efficiency and entrainment of desulfurizing agents/byproducts resulting from FGD systems are specifically discussed for a better comparison of their environmental benefits.

EXPERIMENTAL MATERIALS AND METHODS

Sampling Units. A field study of PM and gaseous pollutants was conducted in five units of typical iron ore sinters equipped with FGD systems and located in two steel and iron factories (labeled F1 and F2). The sintering areas of the three tested sintering machines in F1 were 360 m^2 (S-1), 2 × 180 m^2 (S-2), and 600 m^2 (S-3), while the sintering areas of the two remaining tested sintering machines, located in F2, were 400 m^2 (S-4) and 450 m^2 (S-5). The sampling locations were set at the FGD inlets and stacks of three sintering (sinter-1, 2, 3) in P1, and the stacks of two sintering (sinter-4, 5) in P2, as described in Table 1. The combustion process was almost the same for the five sinters, all of which were equipped with the same ESP structures to collect and recycle dust from the furnaces. Iron-containing raw material (iron ore powder and collected dust from the ESPs), fuel (pulverized coal and coke breeze), and solvent (lime and limestone mixture) were mixed/granulated by adding water and then placed in a sintering device for sintering. During the sintering process, exhaust gases were sucked into bottom bellows through the sintering bed and then entered the ESPs. These exhaust gases passed through the ESPs and FGD systems and were then released into the atmosphere from the stacks. Information about the parameters of sinter ores, desulfurizer agents, and byproducts are detailed in Table S1.

Figure 1 simply illustrates the APCD equipment and sampling sites in the studied sinters. FGD systems were installed between the ESPs and the stacks. The common FGD technologies employed to reduce SO_2 and PM concentrations were limestone WFGD (S-1) combined with WESP, ammonia WFGD (S-2) combined with WESP, activated coke dry FGD (S-3), and semidry CFB-FGD (S-4 and S-5). Field sampling was performed at the inlets of the FGD systems and stacks from August 3rd to September 12th, 2018. The sampling sites were all located in the vertical pipes and were not close to the elbows of the pipes. The working conditions of the five sintering machines were essentially stable, and the operational load was close to full.

Sampling Equipment and Methods. The sampling of PM (or TSP, total suspended particulates) and $PM_{2.5}$ was conducted via an ESC C-5000 isokinetic sampling system (Environmental Supply Company), according to USEPA Method 17 and Method 201A, respectively. The TSP sampling system is a complete set of equipment that meets the requirements of the above two EPA methods. Figure S2a shows the schematic of the sampling equipment based on Methods 17 and 201A; the system consisted of a heated stainless steel sampling probe (with a front isokinetic nozzle to capture TSP or with a $PM_{2.5}$ cyclone to classify and capture $PM_{2.5}$) and a 47 mm stainless steel filter holder for affixing a sampling filter. The isokinetic nozzle/cyclone and sampling probe were heated and maintained at 120 °C to avoid condensation on the sampler walls during sampling. Constant-current isokinetic sampling was performed after predicting the sampling flow rate from the humidity and flue gas flow rate for both TSP and $PM_{2.5}$ sampling. Particles were collected on both quartz fibers (Whatman 1851-865, U.K.) and Teflon filters

DOI: 10.1021/acs.est.9b03081
Environ. Sci. Technol. 2019, 53, 10361−10370

(Whatman 7592-104, U.K.). Some of the sampling particles lost to the inner surface of the filter holder and the cyclone exit tube were collected via rinsing twice with acetone and hexane. The collected rinses were weighed after evaporation in a chemical hood. The duration of each TSP/$PM_{2.5}$ sampling experiment was fixed at 30 min; four samples collected on two quartz-fiber filters and two Teflon filters were successfully sampled at each sampling site. The water content at each sampling site was also simultaneously collected by postpositional water collection trains in the above sampling system. The flue gas with water vapor was successively passed through a spiral tube condenser, dry impingers, and a silica gel impinger (see Figure S2a). After condensation via using ice water, the water in the dry impingers was collected for subsequent weighing analysis to calculate the water content in the flue gas.

Size-segregated PM samples were also collected via a high-temperature DLPI$^+$ (Dekati Low Pressure Impactor, Finland), which classified particles ranging from 16 nm to 10 μm in an aerodynamic diameter into 14 stages on quartz-fiber/Teflon filters 25 mm in diameter (see Figure S2b). A $PM_{2.5}$ cyclone was added to the inlet to remove large particles and droplets. The $PM_{2.5}$ cyclone, sampling, probe and DLPI$^+$ were all heated to 120 °C for avoiding condensation of acidic gaseous species (i.e., SO_3 and HCl) during the sampling. The sampling time was set to 40 min with a flow rate fixed at 10 L/min to ensure adequate particles on filter in every stage of DLPI$^+$. Four successful series of size-segregated PM samples (two series on quartz-fiber filters and two series on Teflon filters) were collected in parallel for each sampling site. Individual primary PMs were also collected on 230-mesh copper transmission electron microscopy (TEM) grids via a single-stage cascade impactor (flow rate 1.0 L/min) connecting a heated sampling probe (120 °C). The preparation and analysis methods of individual PMs were detailed in our previous paper.[27]

A flue gas analyzer (Testo 350, Germany) was employed to monitor gaseous pollutants, including CO, NO, NO_2, and SO_2. The flue gas analyzer was zeroed using standard air before sampling. The gaseous pollutants NH_3 and HCl in the flue gases were also sampled by the ESC C-5000 isokinetic sampling system by adding 50 mL solutions with 30 mmol/L H_2SO_4 and NaOH as absorption solutions, respectively, to two-stage dry impingers, which were soaked in the ice bath with the temperature maintained at <30 °C.[28] The sampling time for the HCl and NH_3 samples was set to 15 min. Figure S2c illustrates the SO_3 sampling system based on Method 8A, consisting of a heating sampling probe, a quartz filter, and a condensing tube. The quartz filter membrane was heated to 260 °C to separate the particles and vaporize the sulfuric acid aerosol. The filtered flue gas passed through the condensing tube at 10 L/min and 80 °C. Gaseous SO_3 and/or H_2SO_4 in the gas was condensed on the tube with no SO_2 condensation. Finally, the collected samples were washed out from the tube with deionized water and saved for further analysis. Three successful absorption samples for each gaseous pollutant (HCl, NH_3, and SO_3) were collected in parallel at each sampling site.

Chemical Analysis and Quality Control. Before each sampling of PMs or gases, the leakage check was performed and the sampling flow rate was also calibrated. All collected filters were weighed by the analytical balance (Sartorius, MSE6.6S-0CE-DM, Germany) in a constant-temperature humidity chamber (50% RH and 20 °C), and the net mass of all valid samples was used to determine the particle mass concentrations in the flue gases. The Teflon filters were used to analyze water-soluble ions (WSIs) and elements, while the quartz-fiber filters were used to analyze organic carbon (OC) and elemental carbon (EC) in the PM samples. Each quartz fiber was preheated at 450 °C for 6 h before sampling. The samples were preserved with a zipper bag in a refrigerator at about −20 °C immediately after collection until gravimetric and chemical analysis.

One-quarter of each Teflon filter was extracted with 10 mL deionized water (resistivity ≥ 18.2 MΩ/cm) for 30 min. The WSIs (K^+, Ca^{2+}, Na^+, Mg^{2+}, NH_4^+, Cl^-, F^-, NO_3^-, and SO_4^{2-}) were examined via an ion chromatograph (940 Professional IC, Metrohm, Switzerland) equipped with a separation column (Metrosep A supp 16-250, Metrohm) and a guard column (Metrosep C6, Metrohm). The concentrations of NH_4^+, Cl^-, and SO_4^{2-} in the field-collected solution samples were analyzed via ion chromatography to determine the concentrations of the gaseous pollutants NH_3, HCl, and SO_3, respectively. The detection limits were within 0.47−3.33 ng/mL. Three successful analyses were performed in parallel for each sample. The remaining three-quarters of each Teflon filter was placed in a digestion vessel, and a mixture of 4 mL HNO_3 (30%) and 1 mL H_2O_2 was added to digest the sample at 170 °C for 4 h. The solutions were diluted to 10 mL with deionized water after cooling. The concentrations of 26 elements (Fe, Si, Al, K, Ca, Cl, S, Mg, Mn, Cd, V, Cr, Ni, Cu, Zn, As, Pb, P, Sn, Sb, Sc, Ti, Co, Se, Br, and Sr) were determined via inductively coupled plasma mass spectrometry (7500a, Thermo).

A punch of 0.508 cm^2 from each quartz-fiber filter was analyzed for OC and EC using a thermal/optical carbon analyzer (Model 2015, Atmoslytic Inc., CA) following the IMPROVE protocol. The sample was successively heated at 140 °C (OC1), 280 °C (OC2), 480 °C (OC3), and 580 °C (OC4) in an anaerobic environment of pure He. A temperature program was employed to sequentially heat the samples to 580 °C (EC1), 740 °C (EC2), and 840 °C (EC3) in a 98% He/2% O_2 atmosphere. The pyrolyzed OC was also detected by calculating the change between the laser reflection signal and the initial value at 580 °C. Detailed descriptions are given elsewhere.[27] The method detection limits for OC and EC were 0.18 ± 0.06 and 0.04 ± 0.01 $\mu g/cm^2$, respectively.

The morphology and components of individual particle samples were analyzed by a field emission high-resolution TEM instrument (JEOL-2100F, Japan) equipped with an Oxford energy-dispersive X-ray spectrometer. To ensure the representativeness of the analyzed particles, three to four areas were selected from the center and periphery of the sampling spot on each grid.

RESULTS AND DISCUSSION

Characteristics of Gaseous Pollutants. Table 1 shows the properties and pollutant concentrations of flue gases from the five stacks after the FGD systems and at the FGD inlets of sinters 1, 2, and 3 in F1; the investigated parameters include SO_2, NO_x, HCl, SO_3, TSP, $PM_{2.5}$, absolute water content, and temperature. The absolute water contents for all tested FGD systems increased during the desulfurizing processes; in particular, the absolute water contents increased by 107 and 121% in the ammonia and limestone WFGDs, respectively, resulting from water evaporation during desulfurization slurry spraying.[5,28] The values in the FGD outlets, according to the FGD technology used, are in the order of dry activated coke < semidry CFB < wet limestone/ammonia FGDs, while the flue gas temperatures are in the reverse order. The reverse order of

DOI: 10.1021/acs.est.9b03081
Environ. Sci. Technol. 2019, 53, 10361−10370

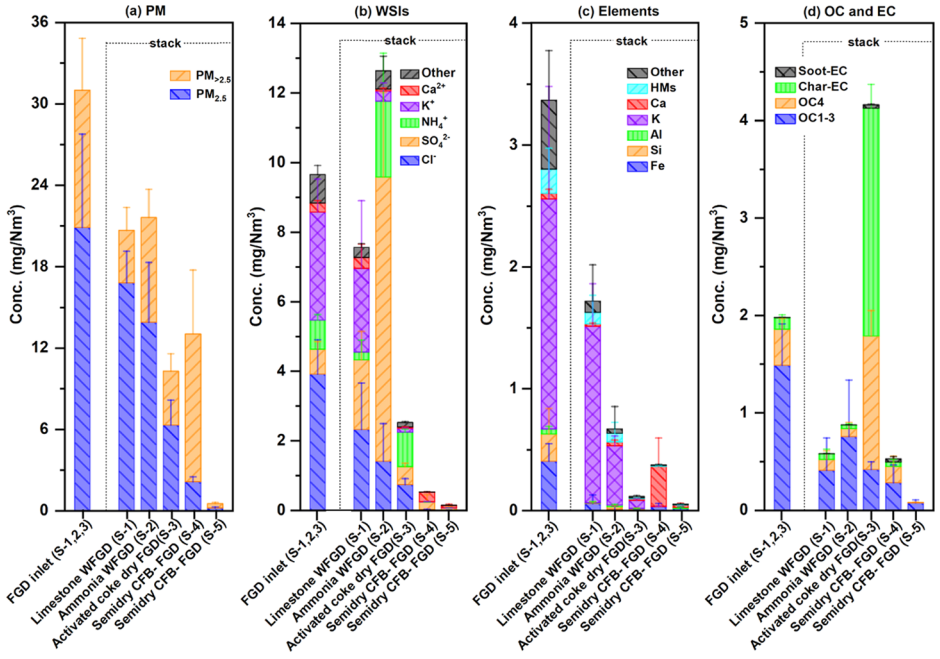

Figure 2. Mass concentrations of PMs (a) and species concentrations in $PM_{2.5}$. WSIs (b), elements (c), and carbonaceous components (d) at the FGD inlets/outlets of the five tested sinters. Note: "Other" WSIs include F^-, Br^-, NO_3^-, Na^+, and Mg^{2+}; HMs include Mn, Cd, V, Cr, Ni, Cu, Zn, As, and Pb; OC1-3 is the sum of OC1, OC2, and OC3; other elements include P, Sn, Sb, Sc, Ti, Co, Se, and Br.

temperatures at the FGD outlets is attributed to heat exchange between the flue gases and the FGD agents/byproducts since FGD devices with higher water consumption have higher heat transfer during the desulfurizing process (see Table S1).

The FGD technology determines not only the water content and temperature of the flue gases but also the concentrations of gaseous pollutants. The desulfurization efficiency of SO_2 ranges from 89.2 to 93.0%, which is lower than that of FGD systems operated in CFPPs (approximately 99%),[5] owing to the lower SO_2 concentrations in sinter FGD inlets. Regarding the fluctuations in and measurement accuracy of flue gases, NO_x concentrations had no obvious change in the FGD systems, except for the activated coke dry FGD system, which used NH_3 and activated coke to synergistically remove NO_x. NO_x decreased by 79.8% after activated coke desulfurization, but the NH_3 concentration increased by 216% to approximately 20 mg/m^3, owing to NH_3 slip, which has commonly been reported in SCR and SNCR systems in CFPPs.[25,29] A higher concentration of NH_3 slip (28.7 mg/m^3) was also found in the outlet of the tested ammonia WFGD system, where NH_3 was used as the desulfurization agent. The removal efficiencies for the other acid gases SO_3 and HCl in wet/dry FGD systems ranged from −323 to 73% and from 96 to 98%, respectively. The SO_3 removal efficiencies are in agreement with those reported for CFPPs, except for that in the ammonia WFGD system.[30] The ammonia WFGD system also increased the SO_3 emission, possibly owing to the decomposition of the desulfurization byproduct ammonium hydrogen sulfate (NH_4HSO_4): $NH_4HSO_4(s) \rightarrow SO_3(g) + NH_3(g) + H_2O(g)$.

Characteristics of Particulate Matter. Two-thirds of the TSP in the FGD inlets is composed of $PM_{2.5}$ (see Table 1), while the TSP in the FGD outlets is affected by the desulfurization process, as shown in Figures 2 and S3. The semidry CFB-FGD equipped with an FF had the highest dust removal efficiency,[31] with average values of 0.54 ± 0.11 and 0.22 ± 0.06 mg/Nm^3 for TSP and $PM_{2.5}$ in the stack for S-5, respectively, while higher concentrations of $PM_{>2.5}$ were observed in the S-4 stack after the semidry CFB-FGD process, possibly owing to the decrease in coarse particle removal efficiency caused by the long service life of the bags (see Table S1). Figures 2b and S3b present the mass concentrations of WSI components in $PM_{2.5}$ at the inlets and the outlets of the FGD systems of the five tested sinters. Cl^- and K^+ (with a proportion close to 1:1; KCl), mainly emitted from the raw sintering materials,[21,32] contributed significantly, accounting for approximately 61.7% of the WSIs in $PM_{2.5}$ at the FGD inlets, but decreased in all FGD systems. The relative concentration of WSIs in $PM_{2.5}$ increased from 46.2% at the FGD inlets to 50.9 and 90.9% at the outlets of the limestone and ammonia WFGD systems, respectively, while decreased to 40.2 and 36.9% for the semidry CFB-FGD and activated coke FGD systems, respectively. The tendency of the limestone WFGD is consistent with that reported for WFGD systems in CFPPs.[5,25] Owing to NH_3 slip, ammonium ion (NH_4^+) dominates the WSI composition as $(NH_4)_2SO_4$ or NH_4HSO_4 in the outlet $PM_{2.5}$ in the FGD systems involving ammonia, such as the ammonia WFGD and the activated coke FGD. Most of the inlet WSI components were removed by above two FGD devices and replaced by desulfurized slurries/byproducts. This phenomenon has also been reported in ammonia WFGDs in CFPPs, owing to the conversion of SO_2 to SO_4^{2-} during FGD processes.[33,34] Similar to the result for the ammonia WFGD, the NH_4^+ mass fraction in TSP and $PM_{2.5}$ after activated coke dry FGD treatment increased by 95.1 and 18.2%, respectively. Along with a high proportion of NH_4^+ (accounting for 16.1 and 15.6% of TSP and $PM_{2.5}$, respectively), the significant increase in SO_4^{2-} in TSP and $PM_{2.5}$ (319 and 1044%) as $(NH_4)_2SO_4$ or NH_4HSO_4 in the ammonia WFGD outlets indicates that desulfurization byproducts are responsible for new particle formation and growth.[5] The SO_4^{2-} in $PM_{2.5}$ also increased by 1.8 times in the limestone FGD outlet, accompanied by an increase of 20% in

DOI: 10.1021/acs.est.9b03081
Environ. Sci. Technol. 2019, 53, 10361−10370

Ca^{2+}, owing to the slip of the desulfurization product (gypsum, $CaSO_4$).[24]

Element analysis confirms the above discussion about the WSI contributions to TSP and $PM_{2.5}$ in the inlets and outlets of the FGD systems, especially K^+, as shown in Figures 2c and S3c. All tested nonvolatile elements (including K, Fe, Al, Si, and heavy metals (HMs)) in TSP and $PM_{2.5}$ exhibited a decreasing tendency in all FGD processes, except for the elements contained in desulfurization agents, such as Ca. Since no nonvolatile elements were used in the activated coke FGD system, all the tested elements significantly decreased by over 70% due to filtration and adsorption by the activated coke. However, the carbonaceous composition of TSP and $PM_{2.5}$ emitted from the activated coke FGD system was significantly increased, accounting for 65.1 and 66.7% of TSP and $PM_{2.5}$, respectively, as shown in Figures 2d and S3d. EC, commonly classified into char-EC and soot-EC according to the IMPROVE-A method,[35] dominated the carbonaceous components of TSP and $PM_{2.5}$ from the activated coke FGD outlet. Char-EC is mainly found in the solid residue after fuel combustion, while soot-EC is formed from volatile substances during high-temperature combustion.[36] Soot-EC and char-EC increased by 62.4 and 18.8 times in the activated coke FGD system, respectively, and are the major components of activated coke, which also contains organic carbonaceous matter, such as OC1-3 and OC4. This phenomenon of the activated coke FGD suggests that a large amount of activated coke was transported out by the flue gas, while the carbonaceous components in other FGD outlets were all decreased in various ratios since desulfurization agents in these FGD systems contain negligible amounts of carbonaceous components.

The TSP concentrations at the outlet of the activated coke dry FGD and semidry CFB-FGD (S-4) were 10.3 ± 1.28 and 13.1 ± 2.45 mg/Nm^3, while those in flue gases from the limestone and ammonia WFGD outlets were 20.7 ± 3.08 and 21.6 ± 5.33 mg/Nm^3, respectively, almost twice as high as those of the dry FGD. As discussed in this section, the chemical compositions and the concentrations of TSP/$PM_{2.5}$ at the tested FGD outlets depend on the deployed FGD technologies.

Particle Compositions According to Desulfurization Agents and Byproducts. FGD systems were revealed to affect the chemical compositions of TSP and $PM_{2.5}$ sampled at the FGD outlets; furthermore, the influence of FGD technologies on particle emissions was systematically evaluated via morphological/chemical investigations of size-segregated particles, as shown in Figures 3, 4, and S4−S6. The mass-based particle size distribution (PSD) in the sub-2.5 μm range at the FGD inlet possesses a unimodal size distribution with a peak at 0.3 μm (see Figure 3), which is the most penetrable size for ESPs and is called the "penetration window".[31,37] This inlet peak is mainly composed of KCl (see Figures 4a and S4). Because of the sweeping mechanism of WFGDs and filtration mechanism of dry/semidry FGDs, particles corresponding to this penetration peak were partially removed in all FGD devices. The PSD profiles at the FGD outlets are very dispersive, but the highest peaks in all PSDs for the FGD outlets shifted to larger sizes for the five tested FGD systems. The PM at the limestone WFGD outlet possesses a three-modal size distribution, consisting of an ultrafine PM mode with a size below 0.1 μm ($PM_{<0.1}$), a fine PM mode from 0.1 to 1 μm ($PM_{0.1-1}$), and a coarse PM mode larger than 1.0 μm

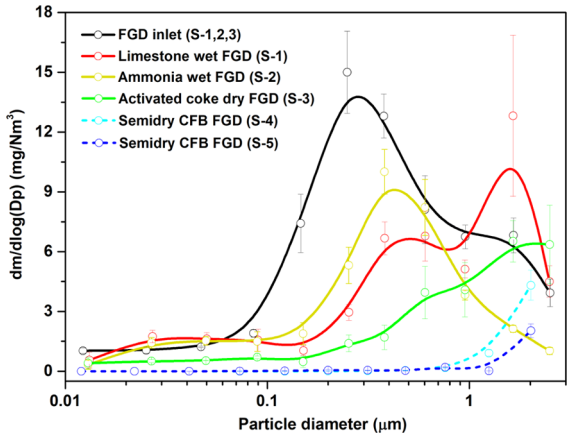

Figure 3. PSDs of PM sampled at the inlets (black line) and the outlets of the five tested FGD systems via high-temperature DLPI+.

($PM_{1-2.5}$). Figure 4a,b, and S5 reveal that the increased emissions for the $PM_{<0.1}$ and $PM_{1-2.5}$ modes are mainly attributed to the additional Ca and SO_4^{2-} contents, as well as the size shift in K and Cl^- from the previous $PM_{0.1-1}$ mode with a peak at 0.3 μm to the coarse mode. These newly generated particulate components mainly originate from desulfurization byproducts escaping from the limestone WFGD system. Comparing the TEM analysis of particles sampled in the stack before and after the FGD system, $CaSO_4$ resembles a rod-like crystal (>1 μm, see Figure S5b) in the limestone WFGD outlet. Additionally, the higher humidity and cooling process in the FGD outlet enhanced particle agglomeration and thus the particle size. Furthermore, the mass ratio of Cl^-/K gradually increased from 1.2 to 3.6 when the particle size increased from 0.15 to 2.46 μm (see Figure 4b), owing to the condensation of volatile Cl^- and gaseous HCl.

Similar to the limestone WFGD process, desulfurization byproducts from the ammonia WFGD system also contribute to the particle composition and mainly include $(NH_4)_2SO_4$ and NH_4HSO_4; furthermore, a bimodal distribution is observed with peaks at 0.03 and 0.4 μm in the PSD, as shown in Figures 3 and 4c. Comparison of the mass fractions of the size-segregated PMs at the FGD inlet (see Figure 4a) shows that the mass fractions of SO_4^{2-} and NH_4^+ contribute significantly to the two peaks, especially at the ~0.4 μm peak, with a contribution of over 90% (see Figure 4c). The newly formed aerosol components likely originated from the entrainment and evaporation of desulfurization byproducts because the sulfate/ammonium mass ratio was between those of $(NH_4)_2SO_4$ and NH_4HSO_4.[38] The particle size at the FGD outlet could be increased when these desulfurization byproducts condense on pre-existing particles. Additionally, the gaseous ammonia volatilized from the desulfurization slurry could be adsorbed by pre-existing particles or could react with SO_2 and be further oxidized to $(NH_4)_2SO_4$ or NH_4HSO_4. The ultrafine-mode particles possibly originate from homogeneous nucleation of the desulfurization byproducts, while the fine-mode particles possibly originate from heterogeneous reactions between the desulfurization byproducts and pre-existing particles from the FGD inlet.

Different from the WFGD results, the PSDs of PM from the semidry CFB-FGD and the dry FGD systems possess a unimodal distribution with a coarse mode peak at >2.5 μm, as

DOI: 10.1021/acs.est.9b03081
Environ. Sci. Technol. 2019, 53, 10361−10370

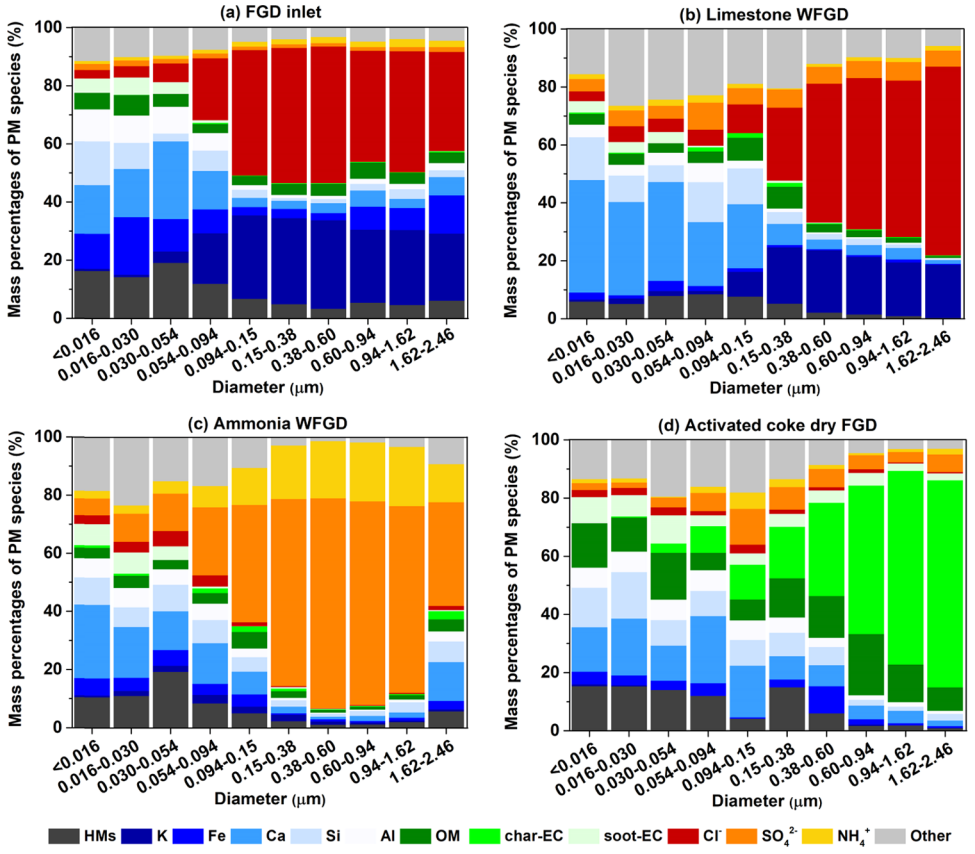

Figure 4. Chemical composition of segregated-size PMs collected at (a) the FGD inlet (S-1,2,3) and 3 stacks after different FGD systems: (b) limestone, (c) ammonia, and (d) activated coke. The PM was sampled via high-temperature DLPI$^+$.

shown in Figure 3. Pre-existing particles from FGD inlets can only survive at the FGD outlets when they successfully penetrate the FFs combined with the CFB-FGD system after avoiding agglomeration with the coarse desulfurizer particles ($Ca(OH)_2$) and desulfurization byproducts ($CaSO_3$ or $CaSO_4$). Thus, most of the fine particles from the FGD inlets were removed in the FGD devices, while the emitted particles are mainly attributed to the escaped coarse desulfurizer particles and their byproducts from the FFs. The PM concentration in the S-4 stack is higher than that in the S-5 stack, mainly owing to the high removal efficiency of all size ranges of PM by the newly installed FFs in S-4. Due to insufficient PM samples collected in each stage of DLPI$^+$ for chemical composition analysis, the effect of the semidry CFB-FGD on the chemical composition of fractional $PM_{2.5}$ is not discussed here. For a similar reason, the activated coke dry FGD device showed a high removal efficiency of pre-existing particles from the FGD inlet via its fluid coke bed. Figures 4d and S6 further show that most of the chemical composition at various size ranges was occupied by activated coke, especially for the larger size range of over 0.6 μm.

FGD systems play at least three vital roles for entering flue gases: (1) reduction of gaseous acid species (including SO_2 and HCl) via adsorption/absorption of desulfurization agents, (2) reduction of PM via collision/adsorption/filtration of desulfurizers/byproducts and/or FGD combined with FF/WESP, and (3) increase in additional PM from desulfurizers and/or FGD reaction byproducts. Therefore, the particles emitted at the stack of these FGD outlets consist of two sources, i.e., the emitted dust from sintering processes and the newly generated particles from the desulfurization byproducts/agents. The characteristics of the increased PM in the stack are determined by the employed FGD technologies and desulfurizers.

Figure S7 shows the variation in $PM_{2.5}$ concentrations and their major species in the limestone WFGD, ammonia WFGD, semidry CFB-FGD, and activated coke dry FGD systems. The primary concentrations of major $PM_{2.5}$ components (including Fe, K, and HMs) only generated from sinters were reduced to different degrees, while the components also contained in FGD desulfurizers/byproducts increased to different degrees. The chemical components in these FGD systems significantly contribute to $PM_{2.5}$ components in the FGD outlets; for example, Ca in limestone wet and semidry FGD systems increases the composition of Ca, NH_4^+ is increased in ammonia WFGD systems, and OC/EC is increased in activated coke dry FGD systems. These results were consistent with previous studies reported on investigating $PM_{2.5}$ emissions from wet and semidry FGD in CFPPs. The proportion of the desulfurization byproducts/agents in $PM_{2.5}$ (about 47.5% limestone and 7.9% gypsum in $PM_{2.5}$) increased in the limestone WFGD outlet on a 300 MW CFPPs before the reform of ultralow-emission.[39] NH_4^+ and SO_4^{2-} generated by the ammonia reaction with SO_2 in the ammonia WFGD process were also reported to be remarkably higher in the PM concentration at the WFGD outlet than that in the inlet.[34] The semidry FGD system also resulted in an increase in some ionic compounds on a 506 MW CFPPs.[40]

Implications for Further Control of PM Emissions. The FGD system, an end-of-pipe technology before the stack

DOI: 10.1021/acs.est.9b03081
Environ. Sci. Technol. 2019, 53, 10361−10370

currently used in the steel and iron industry, determines the emission characteristics of PM to different degrees. WFGD systems carry part of the desulfurization slurry and the water-soluble byproducts, which contribute to the emitted PM concentration after desulfurization and subsequent WESP treatment. Compared to the limestone WFGD, the ammonia WFGD system contributes a higher mass ratio of emitted PMs after desulfurization due to the high solubility of its byproducts and slurry, as well as the heterogeneous byproducts from the reaction between the desulfurizers and acid gaseous species. The semidry and dry FGD systems remove pre-existing particles from the FGD inlets with high efficiency, mainly via physical processes of collision and filtration, while the number of new particles in the FGD devices is directly increased by powders of the desulfurizers and their byproducts.

Figure 5 summarizes the relative contributions of the newly generated components from the FGD systems to PM emissions in the stack. The estimation of newly generated components originating from FGD systems is estimated based on the assumption of the most abundant metal elements (i.e., K and Fe), which are increased by FGD desulfurizers and their byproducts (see the description in the Supporting Information text). Relative mass ratios of 16.5, 63.4, 59.4, and 70.7% in the emitted $PM_{2.5}$ components are replaced by FGD desulfurizers and their byproducts for limestone WFGD, ammonia WFGD, semidry CFB-GFD, and activated coke dry FGD systems, respectively. The 16.5% replaced components of $PM_{2.5}$ in the limestone WFGD outlet are occupied by SO_4^{2-} (9.1%) and Ca (2.3%), while the 63.4% in the ammonia WFGD outlet are dominated by SO_4^{2-} (43.1%) and NH_4^+ (14.2%). The 59.4% increase in components in the CFB semidry FGD outlet was mainly attributed to Ca (22.6%) and SO_4^{2-} (13.1%), and the higher proportions of other compounds may be derived from impurities of the desulfurizer itself or unreacted hydrated lime.

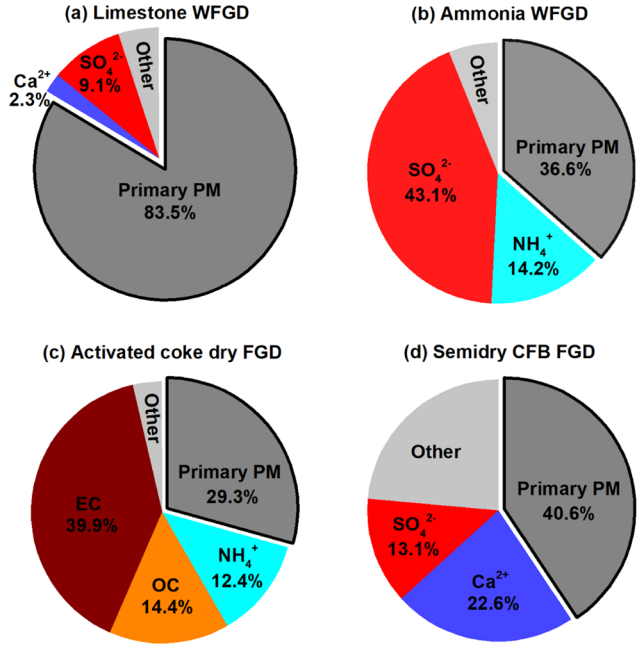

Figure 5. Relative contributions of desulfurization byproducts with major chemical compositions and primary PMs from various FGD processes ((a) limestone, (b) ammonia, (c) activated coke, and (d) CFB) in averaged $PM_{2.5}$ emissions in flue gases at stacks.

The $PM_{2.5}$ in the activated coke dry FGD outlet possesses a high ratio of EC (39.9%), OC (14.4%), and NH_4^+ (14.2%). The proportion of byproducts in $PM_{2.5}$ in the ammonia WFGD, activated coke dry FGD and CFB semidry FGD is over 60%, but this is not the case in the limestone WFGD. The smaller effect on $PM_{2.5}$ component characteristics at the limestone WFGD outlet could be attributed to its relatively mature desulfurization process (optimal size of spraying slurry droplets) and the efficiency of removing entrained droplets of enriched byproducts by its demister and WESP. Limestone WFGD is the dominated technology (about 90%) for reducing SO_2 in CFPPs. Since the concentration of PM is greatly influenced by the scouring intensity of desulfurization slurry and the effect of flue gas carrying. High-efficiency WESP has been commonly installed in front of the stack to effectively reduce the final PM emission to meet the "ultralow-emission standard" in CFPPs recently.[5] Compared to that of CFPPs, more attention about the newly generated components from the FGD systems to PM emissions should be paid for the steel industry.

The replaced PM components in the stacks imply that the installed FGD systems can not only remove PM from FGD inlets with high ratios but also contribute new particles from their agents and byproducts with relatively high ratios. The newly contributed components in PM in the wet and semidry FGDs are dominated by sulfate (SO_4^{2-}), as well as their accompanying cation components (Ca^{2+} and NH_4^+). The increased sulfate emission is likely linked with the key components during heavy haze in China.[41,42] The dry FGD system directly contributes its activated carbon powder to the emitted PM, which possibly increases the negative effect of black-carbon climate forcing issues in the atmosphere.[43] To meet the coming ultralow-emission standard for the steel industry in China, the mature and most commonly used limestone WFGD technology showed the lowest contribution to the final emitted PM. Our results suggest that the deployment of FGD technologies in the steel industry should be comprehensively considered to avoid additional negative impacts from unexpectedly increased PM components.

■ ASSOCIATED CONTENT

Supporting Information

The Supporting Information is available free of charge on the ACS Publications website at DOI: 10.1021/acs.est.9b03081.

Parameters of sinter ores, desulfurizer agents and byproducts; annual steel production and the relative percentages; schematic diagrams of the sampling systems; mass concentrations of TSP and its components; description of estimation method of desulfurization byproducts in PM emitted at the stack (PDF)

■ AUTHOR INFORMATION

Corresponding Authors

*E-mail: qli@fudan.edu.cn. Phone: +86-021-31248901 (Q.L.).
*E-mail: jmchen@fudan.edu.cn. Phone: +86-21-31242298 (J.C.).

ORCID

Qing Li: 0000-0003-0587-1748

Notes

The authors declare no competing financial interest.

DOI: 10.1021/acs.est.9b03081
Environ. Sci. Technol. 2019, 53, 10361−10370

■ ACKNOWLEDGMENTS

This work was supported by the Ministry of Science and Technology of China (2016YFC0202700 and 2018YFC0213800) and the National Natural Science Foundation of China (91743202 and 21876028).

■ REFERENCES

(1) Huang, R. J.; Zhang, Y. L.; Bozzetti, C.; Ho, K. F.; Cao, J. J.; Han, Y. M.; Daellenbach, K. R.; Slowik, J. G.; Platt, S. M.; Canonaco, F.; Zotter, P.; Wolf, R.; Pieber, S. M.; Bruns, E. A.; Crippa, M.; Ciarelli, G.; Piazzalunga, A.; Schwikowski, M.; Abbaszade, G.; Schnelle-Kreis, J.; Zimmermann, R.; An, Z. S.; Szidat, S.; Baltensperger, U.; Haddad, I. E.; Prévôt, A. H. High Secondary Aerosol Contribution to Particulate Pollution During Haze Events in China. *Nature* **2014**, *514*, 218−222.

(2) Moch, J. M.; Dovrou, E.; Mickley, L. J.; Keutsch, F. N.; Cheng, Y.; Jacob, D. J.; Jiang, J.; Li, M.; Munger, J. W.; Qiao, X.; Zhang, Q. Contribution of Hydroxymethane Sulfonate to Ambient Particulate Matter: A Potential Explanation for High Particulate Sulfur During Severe Winter Haze in Beijing. *Geophys. Res. Lett.* **2018**, *45*, 11969−11979.

(3) An, Z.; Huang, R. J.; Zhang, R.; Tie, X.; Li, G.; Cao, J.; Zhou, W.; Shi, Z.; Han, Y.; Gu, Z.; Ji, Y. Severe Haze in Northern China: A Synergy of Anthropogenic Emissions and Atmospheric Processes. *Proc. Natl. Acad. Sci. U.S.A.* **2019**, *116*, 8657−8666.

(4) Liu, X.; Gao, X.; Wu, X.; Yu, W.; Chen, L.; Ni, R.; Zhao, Y.; Duan, H.; Zhao, F.; Chen, L.; Gao, S.; Xu, K.; Lin, J.; Ku, A. Y. Updated Hourly Emissions Factors for Chinese Power Plants Showing the Impact of Widespread Ultralow Emissions Technology Deployment. *Environ. Sci. Technol.* **2019**, *53*, 2570−2578.

(5) Wu, B.; Tian, H.; Hao, Y.; Liu, S.; Liu, X.; Liu, W.; Bai, X.; Liang, W.; Lin, S.; Wu, Y.; Shao, P.; Liu, H.; Zhu, C. Effects of Wet Flue Gas Desulfurization and Wet Electrostatic Precipitators on Emission Characteristics of Particulate Matter and Its Ionic Compositions from Four 300 Mw Level Ultralow Coal-Fired Power Plants. *Environ. Sci. Technol.* **2018**, *52*, 14015−14026.

(6) Li, J.; Qi, Z.; Li, M.; Wu, D.; Zhou, C.; Lu, S.; Yan, J.; Li, X. Physical and Chemical Characteristics of Condensable Particulate Matter from an Ultralow-Emission Coal-Fired Power Plant. *Energy Fuels* **2017**, *31*, 1778−1785.

(7) Zheng, C.; Hong, Y.; Liu, S.; Yang, Z.; Chang, Q.; Zhang, Y.; Gao, X. Removal and Emission Characteristics of Condensable Particulate Matter in an Ultralow Emission Power Plant. *Energy Fuels* **2018**, *32*, 10586−10594.

(8) Liu, X.; Xu, Y.; Zeng, X.; Zhang, Y.; Xu, M.; Pan, S.; Zhang, K.; Li, L.; Gao, X. Field Measurements on the Emission and Removal of $PM_{2.5}$ from Coal-Fired Power Stations: 1. Case Study for a 1000 Mw Ultrasupercritical Utility Boiler. *Energy Fuels* **2016**, *30*, 6547−6554.

(9) Liu, X.; Xu, Y.; Fan, B.; Lv, C.; Xu, M.; Pan, S.; Zhang, K.; Li, L.; Gao, X. Field Measurements on the Emission and Removal of $PM_{2.5}$ from Coal-Fired Power Stations: 2. Studies on Two 135 Mw Circulating Fluidized Bed Boilers Respectively Equipped with an Electrostatic Precipitator and a Hybrid Electrostatic Filter Precipitator. *Energy Fuels* **2016**, *30*, 5922−5929.

(10) Zheng, B.; Tong, D.; Li, M.; Liu, F.; Hong, C.; Geng, G.; Li, H.; Li, X.; Peng, L.; Qi, J.; Yan, L.; Zhang, Y.; Zhao, H.; Zheng, Y.; He, K.; Zhang, Q. Trends in China's Anthropogenic Emissions since 2010 as the Consequence of Clean Air Actions. *Atmos. Chem. Phys.* **2018**, *18*, 14095−14111.

(11) Wu, X.; Zhao, L.; Zhang, Y.; Zheng, C.; Gao, X.; Cen, K. Primary Air Pollutant Emissions and Future Prediction of Iron and Steel Industry in China. *Aerosol Air Qual. Res.* **2015**, *15*, 1422−1432.

(12) Khaparde, V. V.; Bhanarkar, A. D.; Majumdar, D.; Rao, C. V. C. Characterization of Polycyclic Aromatic Hydrocarbons in Fugitive PM_{10} Emissions from an Integrated Iron and Steel Plant. *Sci. Total Environ.* **2016**, *562*, 155−163.

(13) Wang, K.; Tian, H.; Hua, S.; Zhu, C.; Gao, J.; Xue, Y.; Hao, J.; Wang, Y.; Zhou, J. A Comprehensive Emission Inventory of Multiple Air Pollutants from Iron and Steel Industry in China: Temporal Trends and Spatial Variation Characteristics. *Sci. Total Environ.* **2016**, *559*, 7−14.

(14) Oravisjärvi, K.; Timonen, K. L.; Wiikinkoski, T.; Ruuskanen, A. R.; Heinänen, K.; Ruuskanen, J. Source Contributions to $PM_{2.5}$ Particles in the Urban Air of a Town Situated Close to a Steel Works. *Atmos. Environ.* **2003**, *37*, 1013−1022.

(15) Liu, G.; Li, J.; Dan, W.; Hui, X. Chemical Composition and Source Apportionment of the Ambient $PM_{2.5}$ in Hangzhou,China. *Particuology* **2015**, *18*, 135−143.

(16) Hsu, C. Y.; Chiang, H. C.; Chen, M. J.; Chuang, C. Y.; Tsen, C. M.; Fang, G. C.; Tsai, Y. I.; Chen, N. T.; Lin, T. Y.; Lin, S. L.; Chen, Y.-C. Ambient $PM_{2.5}$ in the Residential Area near Industrial Complexes: Spatiotemporal Variation, Source Apportionment, and Health Impact. *Sci. Total Environ.* **2017**, *590*−*591*, 204−214.

(17) Cai, S.; Wang, Y.; Zhao, B.; Wang, S.; Chang, X.; Hao, J. The Impact of the "Air Pollution Prevention and Control Action Plan" on $PM_{2.5}$ Concentrations in Jing-Jin-Ji Region During 2012−2020. *Sci. Total Environ.* **2017**, *580*, 197−209.

(18) Cai, S.; Ma, Q.; Wang, S.; Zhao, B.; Brauer, M.; Cohen, A.; Martin, R. V.; Zhang, Q.; Li, Q.; Wang, Y.; Hao, J.; Frostad, J.; Forouzanfar, M. H.; Burnett, R. T. Impact of Air Pollution Control Policies on Future $PM_{2.5}$ Concentrations and Their Source Contributions in China. *J. Environ. Manage.* **2018**, *227*, 124−133.

(19) Hebei Provincial Department of Ecological Environment. Ultra-Low Emission Standards for Air Pollutants in the Iron and Steel Industry in Hebei Province (in chinese) (DB132169-2018). http://hbepb.hebei.gov.cn/ztbd/dqwrzhzlgj/zywj/201901/t20190108_69334.html (accessed Jan 8, 2019).

(20) Yang, H.-H.; Lee, K.-T.; Hsieh, Y.-S.; Luo, S.-W.; Huang, R.-J. Emission Characteristics and Chemical Compositions of Both Filterable and Condensable Fine Particulate from Steel Plants. *Aerosol Air Qual. Res.* **2015**, *15*, 1672−1680.

(21) Tsai, J. H.; Lin, K. H.; Chen, C. Y.; Ding, J. Y.; Choa, C. G.; Chiang, H. L. Chemical Constituents in Particulate Emissions from an Integrated Iron and Steel Facility. *J. Hazard. Mater.* **2007**, *147*, 111−119.

(22) Menad, N.; Tayibi, H.; Carcedo, F. G.; Hernández, A. Minimization Methods for Emissions Generated from Sinter Strands: A Review. *J. Cleaner Prod.* **2006**, *14*, 740−747.

(23) Wang, X.; Lei, Y.; Yan, L.; Liu, T.; Zhang, Q.; He, K. A Unit-Based Emission Inventory of SO_2, NO_X and PM for the Chinese Iron and Steel Industry from 2010 to 2015. *Sci. Total Environ.* **2019**, *676*, 18−30.

(24) Córdoba, P. Status of Flue Gas Desulphurisation (FGD) Systems from Coal-Fired Power Plants: Overview of the Physic-Chemical Control Processes of Wet Limestone FGDs. *Fuel* **2015**, *144*, 274−286.

(25) Li, Z.; Jiang, J.; Ma, Z.; Fajardo, O. A.; Deng, J.; Duan, L. Influence of Flue Gas Desulfurization (FGD) Installations on Emission Characteristics of $PM_{2.5}$ from Coal-Fired Power Plants Equipped with Selective Catalytic Reduction (SCR). *Environ. Pollut.* **2017**, *230*, 655−662.

(26) Yao, S.; Cheng, S.; Li, J.; Zhang, H.; Jia, J.; Sun, X. Effect of Wet Flue Gas Desulfurization (WFGD) on Fine Particle ($PM_{2.5}$) Emission from Coal-Fired Boilers. *J. Environ. Sci.* **2019**, *77*, 32−42.

(27) Wu, D.; Li, Q.; Ding, X.; Sun, J.; Li, D.; Fu, H.; Teich, M.; Ye, X.; Chen, J. Primary Particulate Matter Emitted from Heavy Fuel and Diesel Oil Combustion in a Typical Container Ship: Characteristics and Toxicity. *Environ. Sci. Technol.* **2018**, *52*, 12943−12951.

(28) Reiter, A. J.; Kong, S. C. Combustion and Emissions Characteristics of Compression-Ignition Engine Using Dual Ammonia-Diesel Fuel. *Fuel* **2011**, *90*, 87−97.

(29) Li, Z.; Jiang, J.; Ma, Z.; Wang, S.; Duan, L. Effect of Selective Catalytic Reduction (SCR) on Fine Particle Emission from Two Coal-Fired Power Plants in China. *Atmos. Environ.* **2015**, *120*, 227−233.

(30) Xu, Y.; Liu, X.; Cui, J.; Chen, D.; Xu, M.; Pan, S.; Zhang, K.; Gao, X. Field Measurements on the Emission and Removal of $PM_{2.5}$

DOI: 10.1021/acs.est.9b03081
Environ. Sci. Technol. 2019, 53, 10361−10370

from Coal-Fired Power Stations: 4. PM Removal Performance of Wet Electrostatic Precipitators. *Energy Fuels* **2016**, *30*, 7465−7473.
(31) Xu, Y.; Liu, X.; Zhang, Y.; Sun, W.; Zhou, Z.; Xu, M.; Pan, S.; Gao, X. Field Measurements on the Emission and Removal of $PM_{2.5}$ from Coal-Fired Power Stations: 3. Direct Comparison on the PM Removal Efficiency of Electrostatic Precipitators and Fabric Filters. *Energy Fuels* **2016**, *30*, 5930−5936.
(32) Guo, Y.; Gao, X.; Zhu, T.; Luo, L.; Zheng, Y. Chemical Profiles of PM Emitted from the Iron and Steel Industry in Northern China. *Atmos. Environ.* **2017**, *150*, 187−197.
(33) Huang, R.; Shi, Y.; Yang, L.; Wu, H.; Pan, D. Aerosol Formation Characteristics During Ammonia-Based WFGD Processes. *Energy Fuels* **2016**, *30*, 9914−9921.
(34) Yan, J.; Bao, J.; Yang, L.; Fan, F.; Shen, X. The Formation and Removal Characteristics of Aerosols in Ammonia-Based Wet Flue Gas Desulfurization. *J. Aerosol Sci.* **2011**, *42*, 604−614.
(35) Han, Y.; Cao, J.; Chow, J. C.; Watson, J. G.; An, Z.; Jin, Z.; Fung, K.; Liu, S. Evaluation of the Thermal/Optical Reflectance Method for Discrimination between Char- and Soot-Ec. *Chemosphere* **2007**, *69*, 569−574.
(36) Han, Y.; Chen, Y.; Ahmad, S.; Feng, Y.; Zhang, G.; et al. High Time- and Size-Resolved Measurements of PM and Chemical Composition from Coal Combustion: Implications for the Ec Formation Process. *Environ. Sci. Technol.* **2018**, *52*, 6676−6685.
(37) Sui, Z.; Zhang, Y.; Peng, Y.; Norris, P.; Cao, Y.; Pan, W.-P. Fine Particulate Matter Emission and Size Distribution Characteristics in an Ultra-Low Emission Power Plant. *Fuel* **2016**, *185*, 863−871.
(38) Pan, D.; Yu, R.; Bao, J.; Wu, H.; Huang, R.; Yang, L. Emission and Formation Characteristics of Aerosols from Ammonia-Based Wet Flue Gas Desulfurization. *Energy Fuels* **2016**, *30*, 666−673.
(39) Wang, H.; Song, Q.; Yao, Q.; Chen, C. Experimental Study on Removal Effect of Wet Flue Gas Desulfurization System on Fine Particles from a Coal-Fired Power Plant. *Proc. Chin. Soc. Electr. Eng.* **2008**, *28*, 1−7.
(40) Saarnio, K.; Frey, A.; Niemi, J. V.; Timonen, H.; Rönkkö, T.; Karjalainen, P.; Vestenius, M.; Teinilä, K.; Pirjola, L.; Niemelä, V.; Keskinen, J.; Häyrinen, A.; Hillamo, R. Chemical Composition and Size of Particles in Emissions of a Coal-Fired Power Plant with Flue Gas Desulfurization. *J. Aerosol Sci.* **2014**, *73*, 14−26.
(41) Cheng, Y. F.; Zheng, G. J.; Wei, C.; Mu, Q.; Zheng, B.; Wang, Z. B.; Gao, M.; Zhang, Q.; He, K. B.; Carmichael, G.; Pöschl, U.; Su, H. Reactive Nitrogen Chemistry in Aerosol Water as a Source of Sulfate During Haze Events in China. *Sci. Adv.* **2016**, *2*, No. e1601530.
(42) Wang, G.; Zhang, R.; Gomez, M. E.; Yang, L.; Levy Zamora, M.; Hu, M.; Lin, Y.; Peng, J.; Guo, S.; Meng, J.; Li, J.; Cheng, C.; Hua, T.; Ren, Y.; Wang, Y.; Gao, J.; Cao, J.; An, Z.; Zhou, W.; Li, G.; Wang, J.; Tian, P.; Marrero-Ortiz, W.; Secrest, J.; Du, Z.; Zheng, J.; Shang, D.; Zeng, L.; Shao, M.; Wang, W.; Y, H.; Wang, Y.; Zhu, Y.; Li, Y.; Hu, J.; Pan, B.; Cai, L.; Y, C.; Ji, Y.; Zhang, F.; Rosenfeld, D.; Liss, P. S.; Duce, R. A.; Kolb, C. E.; Molinax, M. J. Persistent Sulfate Formation from London Fog to Chinese Haze. *Proc. Natl. Acad. Sci. U.S.A.* **2016**, *113*, 13630−13635.
(43) Bond, T. C.; Doherty, S. J.; Fahey, D. W.; Forster, P. M.; Berntsen, T.; DeAngelo, B. J.; Flanner, M. G.; Ghan, S.; Kärcher, B.; Koch, D.; Kinne, S.; Kondo, Y.; Quinn, P. K.; Sarofim, M. C.; Schultz, M. G.; Schulz, M.; Venkataraman, C.; Zhang, H.; Zhang, S.; Bellouin, N.; Guttikunda, S. K.; Hopke, P. K.; Jacobson, M. Z.; Kaiser, J. W.; Klimont, Z.; Lohmann, U.; Schwarz, J. P.; Shindell, D.; Storelvmo, T.; Warren, S. G.; Zender, C. S. Bounding the Role of Black Carbon in the Climate System: A Scientific Assessment. *J. Geophys. Res. Atmos.* **2013**, *118*, 5380−5552.

DOI: 10.1021/acs.est.9b03081
Environ. Sci. Technol. 2019, 53, 10361−10370